Prediction and modelling of doubly-charged ions in the Earth's upper atmosphere

C. Simon, J. Lilensten, O. Dutuit, R. Thissen, O. Witasse, C. Alcaraz, H. Soldi-Lose

Annales Geophysicae, 23, 781–797, 2005
SRef-ID: 1432-0576/ag/2005-23-781

Annales Geophysicae

Prediction and modelling of doubly-charged ions in the Earth's upper atmosphere

C. Simon[1], J. Lilensten[1], O. Dutuit[2], R. Thissen[2], O. Witasse[3], C. Alcaraz[4], and H. Soldi-Lose[2]

[1]Laboratoire de Planétologie de Grenoble, Grenoble, France
[2]Laboratoire de Chimie-Physique, Centre Universitaire, Orsay, France
[3]Research and Scientific Support Department of ESA, ESTEC, Noordwijk, The Netherlands
[4]Laboratoire LURE, Centre Universitaire Paris-Sud, Orsay, France

Received: 18 July 2004 – Revised: 12 January 2005 – Accepted: 28 January 2005 – Published: 30 March 2005

Abstract. We discuss the existence of the doubly-charged ions N_2^{++}, O_2^{++} and O^{++} in the Earth's ionosphere through the theoretical computation of density profiles over the altitude range 100–500 km calculated with the TRANSCAR model. Photoproductions and electron impact productions are described in detail. The photochemical equilibrium assumption verified in this context yields density profiles, validated by comparison to the measurements of the satellite Atmosphere Explorer. Those three dications are lost essentially by dissociative recombination and collisions with the neutrals N_2, O_2 and O. The metastable lifetime of N_2^{++} is 3 s and is estimated at 4 s for O_2^{++}. A survey of the sensitivity to geophysical parameters (solar activity, latitude and solar zenith angle) is also shown. Emphasis is cast on the need for rate constants for chemical reactions involving doubly-charged ions. The fit of the model yields an estimated value of $1.06\pm0.40\times10^{-10}$ cm^3 s^{-1} for the rate constant of the O^{++}+O reaction.

Keywords. Ionosphere (Ion chemistry and composition, Modelling and forecasting, Planetary ionospheres)

1 Introduction

The existence of stable doubly-charged molecular ions in laboratories dates back to the early years of the last century when Aston (1920) and then Thomson (1921) made the first discovery of what was then proposed to be either CO^{++} or N_2^{++}. Half a century later aeronomers finally worked up an interest in the role of dications into the ionosphere: Vegard quoted by Meinel (1951) announced the identification of the OIII line at 500.8 nm in the aurora spectrum for the strong feature observed near 500.04 nm. However, as the 496.0-nm line (which completes the doublet lines for O^{++}) did not appear in the spectrum, the discovery was finally rejected by most authors.

Correspondence to: C. Simon
(cyril.simon@obs.ujf-grenoble.fr)

Nearly at the same time as the lead for a spectral evidence was becoming more and more disputed, Hoffman (1967) reported the detection of O^{++} in the topside ionosphere by the mass spectrometer on board Explorer 31. Several theoretical attempts were then led in the ionosphere (Walker, 1970), as well as in the magnetosphere (Nakada and Singer, 1968; Horwitz, 1981). Many authors such as Prasad and Furman (1975) and above all Avakyan (1978a, b) pointed out the necessity for a theoretical modelling approach to take into account doubly-charged ions, namely N_2^{++}, O_2^{++} and O^{++}. Due to the very large uncertainties concerning the production, stability and reactivity of molecular dications, every effort from this time on converged on the modelling of O^{++} densities in comparison to the few available measurements: in this context, Breig et al. (1977) used Atmosphere Explorer C satellite data recorded in 1974, and with simple assumptions, they produced the very first model of O^{++} densities, though reaction rates still corresponded to fits with experimental data. Only one production reaction was put forward to account for observed densities, i.e. ionisation of O^+. However, one year later, Avakyan (1978a, 1980) and then Victor and Constantinides (1979) showed that another source for O^{++} in the thermosphere had been previously neglected, namely double photoionisation of O, found to be the dominant mechanism below 500 km. Breig et al. (1982) then revised their hypotheses and produced another model that was compared with the same Atmosphere Explorer data for which the processing had been improved. They found good agreement and drew their conclusions on the validity of the reaction rate constants for O^{++}+O, deduced to be k=6.6×10^{-11} cm^3 s^{-1}. However, other studies were conducted at the same time by Fox and Victor (1981) on Venus whose conclusions on reaction rate constants differed from those of Breig et al. (1982) by a factor of two, i.e. k=1.5×10^{-10} cm^3 s^{-1}. Later on, a study of this reaction in Io plasma torus yielded the value 2.0×10^{-10} cm^3 s^{-1} (Brown et al., 1983), which was close to the value of Fox and Victor.

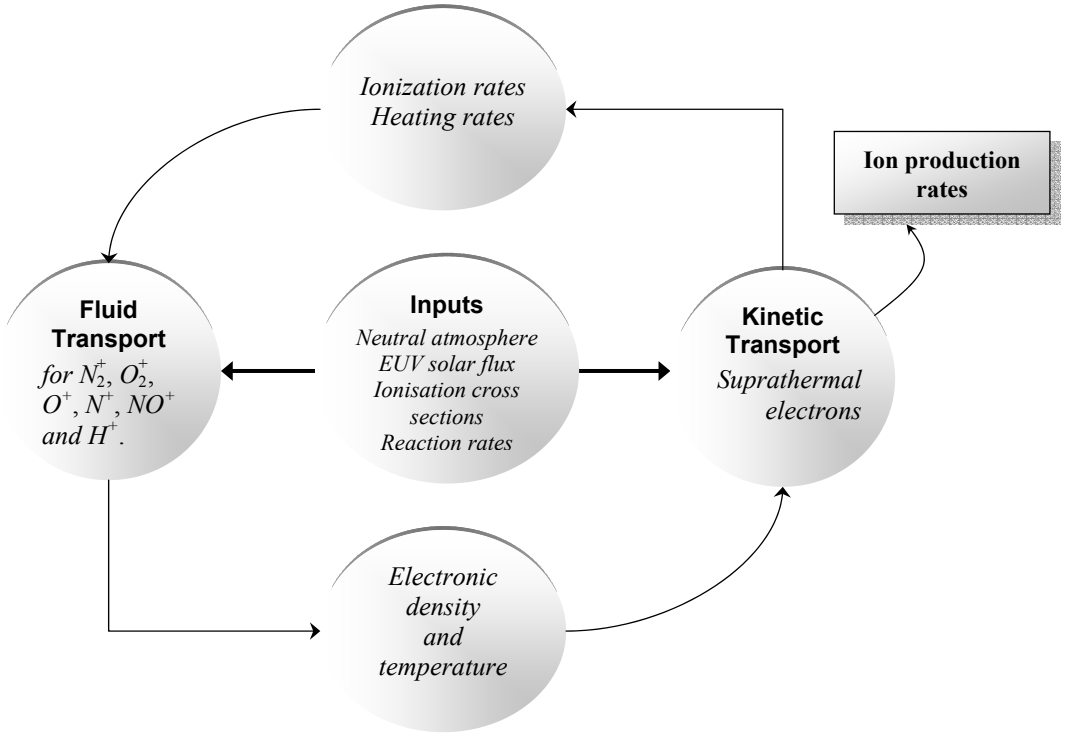

Fig. 1. Synopsis of the fluid/kinetic transport model TRANSCAR. We show only the outputs that are involved in the present study, together with the basic couplings.

Very recently, a period which coincided with the maturity of both the experimental study of dications (see Mrázek et al., 2000 and references therein) and ionosphere models, Witasse et al. (2002, 2003) predicted the existence of a CO_2^{++} layer in the atmosphere of Mars with the ionosphere model TRANSCAR which was specially adapted to the Martian conditions (Witasse, 2000; Morel et al., 2004).

With the growing possibilities of high-resolution measurements made by satellites and ground-based facilities, we will have access to more and more ionospheric parameters: we present here the first complete computation of N_2^{++}, O_2^{++} and O^{++} ion densities in the Earth's upper atmosphere.

We first describe the photochemical model and focus our description on the production's computation, both primary and secondary, and the loss processes taken into account for each ion. Dication densities are then deduced.

The second part deals with the inputs of the model, i.e. cross sections, extreme ultra-violet (EUV) solar flux and the neutral atmosphere. In the third section we show the results of the modelling and validate the model by a comparison with Atmosphere Explorer data. We can then detail the steps of the computation which yields interesting features while modifying geophysical parameters.

The last paragraph addresses the possibility of detection of such ions applied to the Earth's upper atmosphere and other planets or satellites in the solar system, notably Titan.

2 The model TRANSCAR applied to dications

The model TRANSCAR and its outputs are described in detail in Lilensten and Blelly (2002). The model describes the upper atmosphere between 90 and 3000 km, assuming it is composed of six ions, namely N_2^+, O_2^+, O^+, N^+, NO^+ and H^+. To summarize, TRANSCAR is a coupled kinetic/fluid model which solves sequentially the Boltzmann kinetic equation for suprathermal electrons and the Boltzmann momentum equations for the 6 ions listed above. Each part is linked with the other and updated through ionisation and heating rates (produced by the kinetic transport code), on the one hand, and through electronic density and temperature yielded by the 1-D, time-dependent fluid transport model, on the other hand (Fig. 1).

For the ion productions which are the outputs of interest in the present study, two mechanisms are taken into account. First, the primary production is the ionisation of the thermosphere due to the solar EUV flux and is basically related to a Beer-Lambert law. Following this first photoproduction, sufficiently high-energy primary electrons may be released that can ionize, in turn, the neutral gas: secondary electrons and ions are then generated, called the secondary ion production. In the latter case, we have to use a physical description in terms of a kinetic transport of suprathermal electrons, given by the kinetic part of TRANSCAR. The Auger effect, originally proposed as a low-altitude source of O^{++} ions by Avakyan (1978a, 1980), is not taken into account here.

The ionisation thresholds of N_2, O_2 and O, for single and double ionisation processes are listed in Table 1. The kinetic formalism described below is relevant to doubly-charged ions, and follows closely the singly-charged ion description of Lilensten and Blelly (2002). The photochemical description proposed in Sect. 2.4 is, however, specific to doubly-charged ions while singly-charged ion parameters are given by the Boltzmann fluid formalism.

2.1 Primary productions

The expression of the primary production profile $P^j_{prim}(z)$ of an ion j is given in $\mathrm{cm^{-3}\,s^{-1}}$ by a simple Beer-Lambert law for the energy E and at the altitude z:

$$P^j_{prim}(z) = n_s(z) \int \sigma_i^{s\rightarrow j}(E)\, I_\infty(E)\, e^{-\tau_{hv}(z,E)}\, dE\,, \qquad (1)$$

where $I_\infty(E)$ is the solar flux on the top of the ionosphere, $\sigma_i^{s\rightarrow j}(E)$ the photoionisation cross section of species s producing the doubly-charged ion j, and $n_s(z)$ the density of the mother species s which can be either a singly-charged ion or a neutral.
$\tau_{hv}(z,E)=\sum_s \sigma_s^a(E) \int_z^\infty n_s(z')\, chap\chi(z')\, dz'$ represents the optical depth, a function of the absorption cross section of the species s noted $\sigma_s^a(E)$ and $chap\chi(z)$, the Chapman function, a function of the altitude and the solar zenith angle χ.

2.2 Kinetic transport and secondary productions

The primary electrons can be of a high enough energy to ionize as well the neutral gas, even for doubly-charged ions, which have a high ionisation threshold. The steady-state kinetic transport equation describes the angular and energy redistributions of electrons and connects the spatial evolution of the electron flux from the top of the ionosphere to the low E-region. Mathematically speaking, when reviewing losses and sources, we can write (Lilensten and Blelly, 2002):

$$\mu \frac{\partial I(\tau,E,\mu)}{\partial \tau(z,E)} = -I(\tau,E,\mu) + sf(\tau,E,\mu) + \frac{n_e(z)}{\sum_k n_k(z)\sigma_k^T(E)} \frac{\partial (L(E)\, I(\tau,E,\mu))}{\partial E} +$$

$$\sum_l \left\{ \frac{n_l(z)\sigma_l^T(E)}{\sum_k n_k(z)\sigma_k^T(E)} \int_{-1}^{1} d\mu' \int_E^\infty dE' R^l(E';\mu\rightarrow E;\mu) I(\tau,E',\mu') \right\}, \qquad (2)$$

where $I(\tau,E,\mu)$ is the electron stationary flux ($\mathrm{cm^2\,s^{-1}\,eV^{-1}\,sr^{-1}}$), E, E', μ and μ' the energies in eV of scattered and incident electrons and their respective pitch-angles cosine. $\sigma_k^T(E)$ stands for the total elastic and inelastic collisions' cross section for the neutral species s, while $n_k(z)$ and $n_e(z)$ represent the density of the neutral species k and the electron density. $\tau(z,E)$ is the electron scattering depth, defined as $d\tau(z,E)=-\sum_s \sigma_k^T(E)\, n_k(z)\, dz$.

Table 1. Ionisation thresholds for some common species.

Species	Single Ionisation threshold (eV)	Double ionisation threshold (eV)	
N_2	15.58	43.00	(Ahmad, 2002)
O_2	12.08	36.13	(Hall et al., 1992)
O	13.61	48.74	(He et al., 1995)
O^+	35.13		

R^l is the redistribution function (or normalized differential cross section) from an initial state (E', μ') to a final state (E, μ) for the neutral species l. It depends on the elastic and inelastic cross sections. The source function $sf(\tau,E,\mu)$, which corresponds to the photoelectron production rate, varies with the precipitated flux or the primary photoelectron flux conditions. The continuous energy loss function $L(E)$, describing the energy transfer from the suprathermal "hot" electrons to the ambient electrons, is computed via a scheme given by Swartz and Nisbet (1972).

The secondary production of the ion j is then:

$$P^j_{\mathrm{sec}}(z) = 2\pi\, n_s(z) \int_{-1}^{1} d\mu \int_0^\infty \sigma_{ie}^{s\rightarrow j}(E)\, I(\tau,E,\mu)\, dE\,. \qquad (3)$$

$\sigma_{ie}^{s\rightarrow j}$(E) is here the electron-impact ionisation cross section for the production of a doubly-charged ion j through the mother species s, either an ion or a neutral.

The final overall production for the doubly-charged species j is simply the sum of the primary and the secondary productions.

$$P^j_{tot}(z) = P^j_{prim}(z) + P^j_{\mathrm{sec}}(z) \qquad (4)$$

2.3 Loss mechanisms for dications: a chemical model

The chemical loss profiles are defined as:

$$L_j(z) = \sum_i k_i\, n_i(z) \;+\; \frac{1}{\tau_j^d}\,, \qquad (5)$$

where k_i is the reaction rate constant ($\mathrm{cm^3\,s^{-1}}$) corresponding to the reaction of N_2^{++}, O_2^{++} or O^{++} with a neutral of density n_i, and τ_j^d is the dissociation lifetime of the molecular doubly-charged ion j.

The electronic recombination rate with $N_2^{++}$is taken from Seiersen et al. (2003). The rate constants for the reaction of O_2^{++} with N_2 and O_2 are taken from Chatterjee and Johnsen (1989). N_2^{++} reaction rate constants are given by new laboratory measurements from the LCP/LURE team with the CERISES apparatus (acronym for Collisions Et Réactions

Table 2. . A comprehensive list of reaction rate constants for N_2^{++}, O_2^{++}, and O^{++} corresponding to the reactions with the neutrals N_2, O_2, O and the electronic recombination.

Species	Reaction	Reaction rate constants ($cm^3\ s^{-1}$)	References
$\mathbf{N_2^{++}}$	$N_2^{++} + N_2 \rightarrow products$	$\boldsymbol{k_1} = 2.70 \times 10^{-9} \pm 25\%$	This work
	$N_2^{++} + O_2 \rightarrow products$	$\boldsymbol{k_2} = 2.80 \times 10^{-9} \pm 25\%$	This work
	$N_2^{++} + e^- \rightarrow N_2^+ + hn$	$\boldsymbol{k_3} = 5.8 \times 10^{-7} \left(\frac{300}{T[K]}\right)^{0.5} \pm 20\%$	Seiersen et al. (2003)
$\mathbf{O_2^{++}}$	$O_2^{++} + N_2 \rightarrow O_2^+ + N_2^+$	$\boldsymbol{k_4} = 2.0 \times 10^{-9}$	Glosik et al. (1978)
		$\boldsymbol{k_4} = (2.0 \pm 0.5) \times 10^{-9}$ *at* 0.04 eV	Chatterjee and Johnsen (1989)
	$O_2^{++} + O_2 \rightarrow O_2^+ + O_2^+$	$\boldsymbol{k_5} = (2.0 \pm 0.5) \times 10^{-9}$ *at* 0.04 eV	Chatterjee and Johnsen (1989)
$\mathbf{O^{++}}$	$O^{++} + N_2 \rightarrow products$ $\boldsymbol{k_6}$	2.9×10^{-10}	Breig et al. (1977)
		$(1.3 \pm 0.3) \times 10^{-9}$ *at* 300 K	Johnsen and Biondi (1978)
		$(1.6 \pm 0.6) \times 10^{-9}$	Howorka et al. (1979)
		1.4×10^{-9}	Geiss and Young (1981)
		$(3.15 \pm 0.26) \times 10^{-9}$ *at* 2×10^4 K	Fang and Kwong (1995)
	$O^{++} + O_2 \rightarrow products$ $\boldsymbol{k_7}$	$(1.5 \pm 0.3) \times 10^{-9}$ *at* 300 K	Johnsen and Biondi (1978)
		$(1.7 \pm 0.7) \times 10^{-9}$	Howorka et al. (1979)
	$O^{++} + O \rightarrow O^+ + O^+$ $\boldsymbol{k_8}$	$1.0 \times 10^{-11} \pm 40\%$	Breig et al. (1977)
		$\sim 2 \times 10^{-11}$	Avakyan (1978*a*)
		$\leq 10^{-10}$	Victor and Constantinides (1979)
		1.5×10^{-10} (in the case of Venus)	Fox and Victor (1981)
		6.6×10^{-11}	Breig et al. (1982)
		2.0×10^{-10} (in the case of Io)	Brown et al. (1983)
		$(1.06 \pm 0.40) \times 10^{-10}$	This work (see text)
	$O^{++} + e^- \rightarrow O^+ + hn$	$\boldsymbol{k_9} = 2.1 \times 10^{-11}\ Z^2\ T^{-0.5}$	Nakada and Singer (1968)
	$O^{++} + N_2 \rightarrow O + N_2^{++}$	$\boldsymbol{k_{10}} \sim 6.8 \times 10^{-11}$	Avakyan (1978*a*)
	$O^{++} + O_2 \rightarrow O + O_2^{++}$	$\boldsymbol{k_{11}} \sim 2 \times 10^{-11}$	Avakyan (1978*a*)

d'Ions Sélectionnés par des Electrons de Seuil). The experimental procedure is described in Nicolas et al. (2002) and Franceschi et al. (2003).

In the case of N_2^{++}, the lifetime of the ion ground state is 3 s (Mathur et al., 1995). For O_2^{++}, as no data is currently available, we assume that the lifetime is limited by the tunnelling through a barrier towards dissociation and we estimate it equal to the lifetime of CO_2^{++}, i.e. 4 s (Mathur et al., 1995). When produced in excited states (electronic or vibrational), the lifetime of the dication is known to decrease rapidly (Cox et al., 2003). Therefore, another unknown is the relative abundance of the dication ground state to the excited states in the "ionisation cross section measurements" reported in Table 3. This is unknown, but as the lifetime is rapidly decreasing with internal energy, and as the spectrometers used for absolute measurement are generally sensitive to species stable in the 10-microseconds-or-more time range, we estimated that the abundance of the ground state might well be 50–80% of the population that was measured. However, as we don't know more precisely the ratio, we chose to use the data from Table 3 as it is, and therefore produce an upper estimate of the expected density of the molecular dications O_2^{++}.

Table 3. Cross sections available for the ionisation of N_2, O_2 and O.

Species	Photoionisation cross section	Maximum cross section value measured (cm^2)		Electron-impact cross section
$N_2 \rightarrow N_2^{++}$	–		3.6×10^{-18}	Halas and Adamczyk (1972)
			3.35×10^{-18}	Märk (1975)
			$\sim 6.6 \times 10^{-18}$	Krishnakumar and Srivastava (1990), maximum estimate*
			$\sim 6.9 \times 10^{-18}$	Straub et al. (1996), estimated*
$O_2 \rightarrow O_2^{++}$	–		1.07×10^{-18}	Märk (1975)
			$\sim 1.9 \times 10^{-18}$	Krishnakumar and Srivastava (1992), maximum estimate*
			$\sim 1.6 \times 10^{-18}$	Straub et al. (1996), estimated*
$O \rightarrow O^{++}$	Angel and Samson (1988)	0.22×10^{-18}	5.56×10^{-18}	Ziegler et al. (1982)
	Fennelly and Torr (1992)	0.22×10^{-18}	5.59×10^{-18}	Zipf (1985)
			5.5×10^{-18}	Itikawa and Ichimura (1990)
$O^+ \rightarrow O^{++}$	Baluja and Zeippen (1988) †	8.50×10^{-18}	43.8×10^{-18}	Aitken & Harrison (1971)
	Kjeldsen et al. (2002) †	8.50×10^{-18}		
	Aguilar et al. (2003) †	10.6×10^{-18}	45.3×10^{-18}	Yamada et al. (1988)

∗ The original measurements concerned the products $N^+ + N_2^{++}$ and $O^+ + O_2^{++}$ together. Maximum estimates on cross sections for the production of N_2^{++} and O_2^{++} are made here on the following assumptions proposed by Krishnakumar and Srivastava (1990) for N_2^{++} and by Märk (1975) for O_2^{++}. According to these authors, a maximum of 10% of the overall $N^+ + N_2^{++}$ production reported may be of N_2^{++} origin while Märk (1975) reports than O_2^{++} cross sections are less than 1% of those for the production of O_2^+, yielding the estimates shown in Table 3.

† Cross sections measured at threshold.

Owing to the existence of measurements of the rate constants for the reaction of O^{++} with N_2, O_2 (discussed in Sect. 4), and O, we can roughly estimate the effective lifetime of O^{++} in multiplying by the corresponding neutral densities $\frac{1}{k_i n_i}$: we obtain an O^{++} lifetime of less than 100 s at all altitudes between 100 and 500 km.

Other loss reactions, namely that of O^{++} with He and H, can be of importance above 600 km, where He and H concentrations become high and rate constants reach values of 1.1×10^{-10} cm^3 s^{-1} for 1000 K. Because all densities are calculated below 500 km, as showen in Sect. 2.4, these loss reactions are assumed to be negligible.

2.4 Output of the model: densities of N_2^{++}, O_2^{++} and O^{++}

Using the continuity equation $\frac{\partial n_j(z)}{\partial t} + \mathrm{div}(n_j(z)\, v_j(z)) = P_j(z) - n_j(z) L_j(z)$, we are now able to determine the density profile of a doubly-charged ion.

The density $n_j(z)$ of a doubly-charged ion j is simply given by the photochemical equilibrium:

$$n_j(z) = \frac{P_{tot}^j(z)}{L_j(z)} \,. \tag{6}$$

This expression is valid at low altitudes, i.e. at altitudes less than 500 km. At higher altitudes, the velocity may become too large to insure the validity of the steady-state assumption.

3 Inputs of the model

To solve Eqs. (1) and (3), we need to know the parameters $n_s(z)$, $\sigma_i^{s \rightarrow j}(E)$, $\sigma_{ie}^{s \rightarrow j}(E)$, and $I_\infty(E)$.

The neutral compositions and temperature are provided by the semi-empirical model MSIS-90 (Hedin, 1987, 1991)

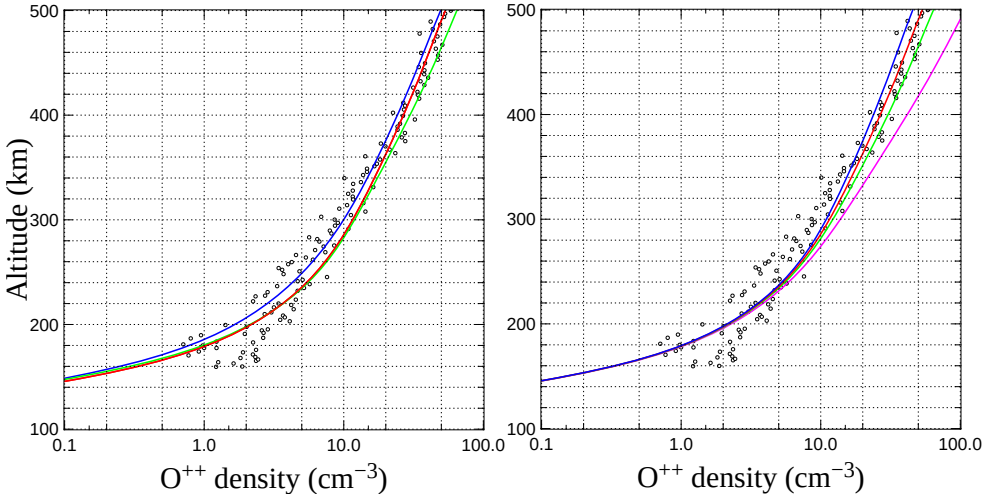

Fig. 2. Left: O^{++} density as recorded by AE-C2758 on 12 August 1974 (circles) and for different geophysical conditions computed by the model in the photoequilibrium assumption (curves). The blue curve stands for the satellite latitude/longitude position (–5.81°,64.87°) for χ=79.99° at altitude 161 km. The red curve corresponds to (–31.55°,54.64°), χ=78.53° at 377 km. The green curve is for the position (–45.67°,45.70°), χ=78.91° at 494 km. Right: evolution of O^{++} density under the variation of the reaction rate constant k_8 (see text) in parallel with AE-C data plots (empty circles). Blue curve: k_8=1.50×10^{-10} cm^3 s^{-1}. Green curve: k_8=1.00×10^{-10} cm^3 s^{-1}. Magenta curve: k_8=5.00×10^{-11} cm^3 s^{-1}. The best fit with AE-C 2758 at χ=78.53° is obtained for k_8=1.25×10^{-10} cm^3 s^{-1}(red curve).

while we use the solar flux model EUV91 with its 39-energy box scheme (Tobiska, 1991) on which the photoionisation cross sections are sampled.

The different ionisation cross sections of interest in this study are summarized in Table 3. Generally speaking, no data have been available up to now for the double photoionisation of the N_2 and O_2 molecules, while for the electron impact, a large documentation exists. The only complete set of data is for O^{++}, for both photoionisation and electron impact ionisation. We use Fennelly and Torr (1992) for double photoionisation of oxygen, and Zipf (1985) for the electron-impact cross section because of their remarkably precise tables.

We take N_2 and O_2 electron-impact double-ionisation cross sections from Märk (1975): it is the only measurement available so far where the direct production of N_2^{++} is given without any spectrometric overlapping with N^+. The double photoionisation of N_2 and O_2 is a more complex source of concern as no results have been published yet. We use the approximation:

$$\frac{\sigma_{h\nu}^{N_2}(N_2^{++})}{\sigma_{h\nu}(N_2)} = \frac{\sigma_e^{N_2}(N_2^{++})}{\sigma_e(N_2)} \quad \text{and}$$
$$\frac{\sigma_{h\nu}^{O_2}(O_2^{++})}{\sigma_{h\nu}(O_2)} = \frac{\sigma_e^{O_2}(O_2^{++})}{\sigma_e(O_2)} \qquad (7)$$

to yield the double photoionisation cross sections $\sigma_{h\nu}^{N_2}(N_2^{++})$ and $\sigma_{h\nu}^{O_2}(O_2^{++})$, where $\sigma_{h\nu}(i)$ stands for the photoabsorption cross section of the neutral species i, $\sigma_e(j)$ or the total electron impact diffusion cross section of the species j and $\sigma_e^i(i^{++})$ for the double electron impact ionisation cross section of the neutral i.

Another source of molecular dications might be the single electron-impact ionisation of N_2^+ and O_2^+: though the ionisation cross sections (of the order of 10^{-17} cm^2 for N_2^+ according to Bahati et al., 2001) is not negligible, the N_2^+ and O_2^+ densities are much smaller than the neutral ones by a factor of at least 10^6. The result is that this contribution to N_2^{++} and O_2^{++} productions is negligible in our context, especially in the low-altitude regions considered here.

4 Validation of the model

In this section, we compare the results of the model described above for O^{++} with the lone experimental data from the magnetic ion mass spectrometer MIMS (Hoffman et al., 1973) on board Atmosphere Explorer (AE), which were recorded 30 years ago (Breig et al., 1982).

4.1 Calculated O^{++} densities compared with AE-C data

The AE satellite sampled data during descent in late afternoon in the southern winter non-polar ionosphere, corresponding to orbits C-2735, C-2743, C-2754, C-2757, C-2758. The solar zenith angle ranged between 75° and 85°, while the magnetic indices A_p remained around 16.

In Fig. 2, we plot O^{++} densities as a function of altitude. On the left panel, we compare AE-C measurements to the model's predictions for three different geographical coordinates, corresponding to data recorded at low altitude (161 km), mean altitude (377 km) and high altitude (594 km). The model reproduces well the data profiles, however, with a little discrepancy between 140 and 200 km: as the measurement uncertainties are also growing larger at these altitudes,

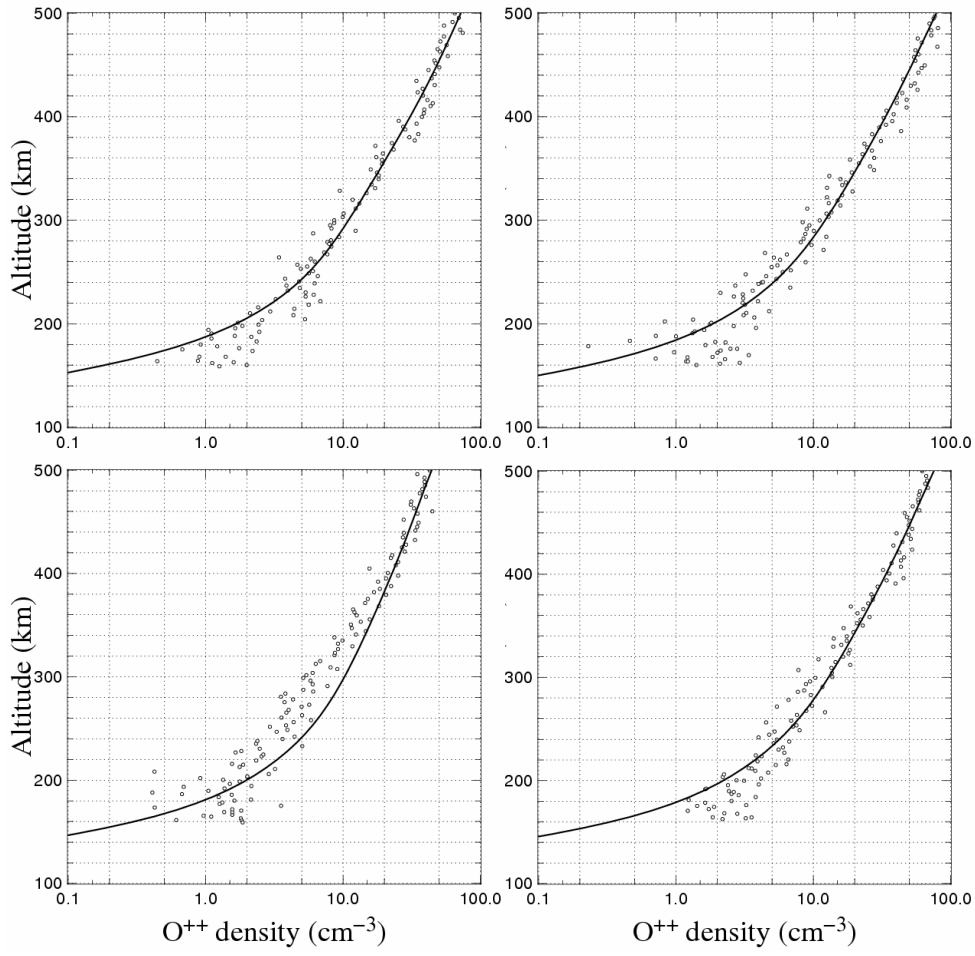

Fig. 3. O^{++} density in the range 100–500 km for AE-C successive orbits 2735 (top left), 2743 (top right), 2754 (bottom left) and 2757 (bottom right). The results of the model are compared to AE–C data and we fit for each plot the reaction rate constant k_8. Top left: k_8=1.1×10^{-10} cm^3 s^{-1}. Top right: k_8=6.5×10^{-11} cm^3 s^{-1}. Bottom left: k_8=1.6×10^{-10} cm^3 s^{-1}. Bottom right: k_8=7.0×10^{-11} cm^3 s^{-1} (AE–C data taken from Breig et al., 1982).

it results in a high spreading of experimental AE data points, which eventually enables one to validate our results at lower altitudes.

In the following subsections, we adopt for the model the average-altitude parameters of each satellite orbit, i.e. for orbit C-2758 χ=78.53°, and the latitude/longitude set (–31.55°, 54.64°), taken as mean conditions.

Let us now discuss our model inputs. As stated above, we use the semi-empirical model MSIS-90 for the neutral atmosphere. This model is in fairly good agreement up to 400 km with the recorded AE-C data for the neutrals. Above 400 km, it clearly overestimates the measurements and reaches a density value higher by a factor of two at 500 km. Nevertheless, depending on the neutral composition inputs (either MSIS or AE-C neutral composition recording), the results of our dication density model are not significantly modified at these high altitudes (differences up to 10% at most). We obtain once more good agreement with AE-C O^{++} density profiles.

We can now test the reaction rate constants listed in Table 2. The best agreement with AE-C O^{++} profiles is

Table 4. Summary of the reaction rate constants obtained for the reaction O^{++}+O on each AE orbit.

AE-C orbit	**Loss rate k_8** (cm^3 s^{-1})
2735	1.10 × 10^{-10}
2743	6.50 × 10^{-11}
2754	1.60 × 10^{-10}
2757	7.00 × 10^{-11}
2758	1.25 × 10^{-10}
Average	(1.06 ± 0.40) × 10^{-10}

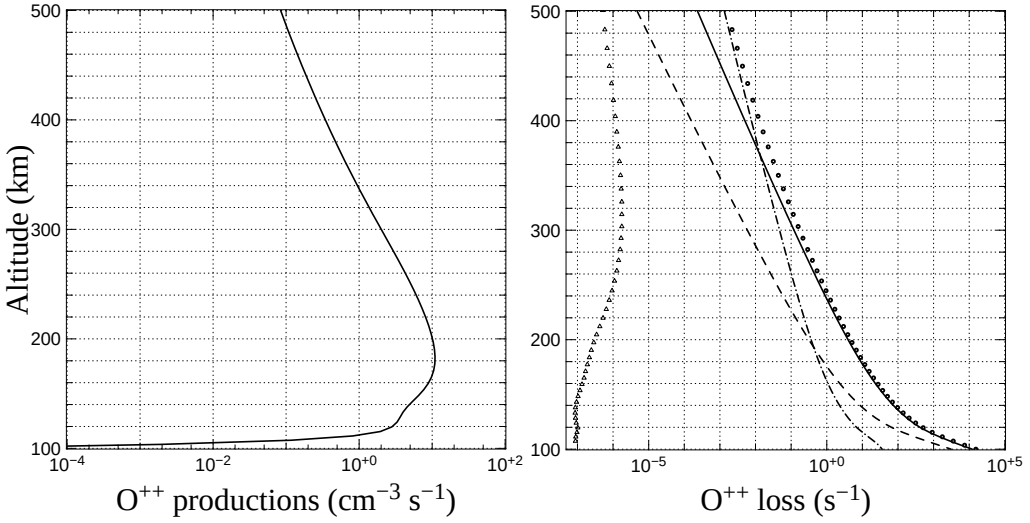

Fig. 4. O^{++} production and loss profiles for orbit 2758. Left panel: total O^{++} production profile. Right panel: loss mechanisms taken into account in the model. Collisions with N_2 (solid curve), with O_2 (dashed curve), with O (dash-dotted curve) and with the electrons (triangles) are represented. The sum of all contributions is in full circles.

Table 5. Set of geophysical parameters used in the model.

Parameters	
Latitude	Tromsø 69.66° *N*, 18.95° *E* Grenoble 45.11° *N*, 5.43° *E*
Solar zenith angle c	$c = 0 - 90°$
Solar activity $f_{10.7}$	$f_{10.7} = 68$ $f_{10.7} = 243$
Magnetic index A_p	$A_p = 3$

found when using the k_6 and k_7 rate constants obtained in laboratory measurements by Howorka et al. (1979). As for the charge-exchange reaction O^{++}+O, which has not been measured but has been derived from models, we are compelled to search for the best fit of our model while varying the coefficient k_8. This is shown in Fig. 2 (right panel) for orbit C-2758: we find the best fit for the value k_8=1.25×10^{-10} cm^3 s^{-1}.

4.2 Determination of the O^{++}+O reaction rate constant

Breig et al. (1982) published AE-C data for different orbits corresponding to the two days before orbit C-2758. They occur in slightly different conditions. The satellite recordings occur during descents that spread from 10 August (C-2735) to 12 August 1974 (C-2757). We plot in Fig. 3 the O^{++} density with the reaction rates defined in the previous section for each satellite orbit. We fit the reaction rate k_8 for each particular recording in order to obtain the best correlation.

These different sets of orbital data lead us to the consensus value $\bar{k}_8$=1.06±0.40×10^{-10} cm^3 s^{-1} at 1σ for the O^{++}+O reaction.

The values fitted are summarised in Table 4 and averaged over the five orbits considered, and eventually yield the coefficient $\bar{k}_8$.

This result ranges nicely in between the extreme values found by Fox and Victor (1981) determined on Venus, i.e. k_8=1.5×10^{-10} cm^3 s^{-1}, and Breig et al. (1982) on Earth, i.e. k_8=6.6×10^{-11} cm^3 s^{-1}. A limitation to these comparisons is that, together with the approach presented here, both authors fitted their model with experimental data while using very simple assumptions for the computation of productions and losses. According to Smith and Adams (1980), Breig et al. (1977) may have well underestimated their values in light of what is expected experimentally for other doubly-charged ions such as Xe^{++} or Ar^{++}, and should be of the order of 10^{-10} cm^3 s^{-1}.

The value retained here needs of course further confirmation from laboratory studies. What's more, the temperature dependence of the reaction rate constant k_8 has to be cleared up as we observe large variations depending on the orbit of the satellite. These variations, though certainly not entirely, could partly be of thermal origin.

4.3 Production and loss profiles for AE-C 2758

In Fig. 4, we plot the O^{++} production and loss profiles for AE orbit No. 2758. On the left panel, the production shows a broad peak that maximizes at 10 ion cm^{-3} s^{-1}near 180 km. On the right panel, we have the detailed contributions of O^{++} losses due to collisions with the neutral gas and the electrons.

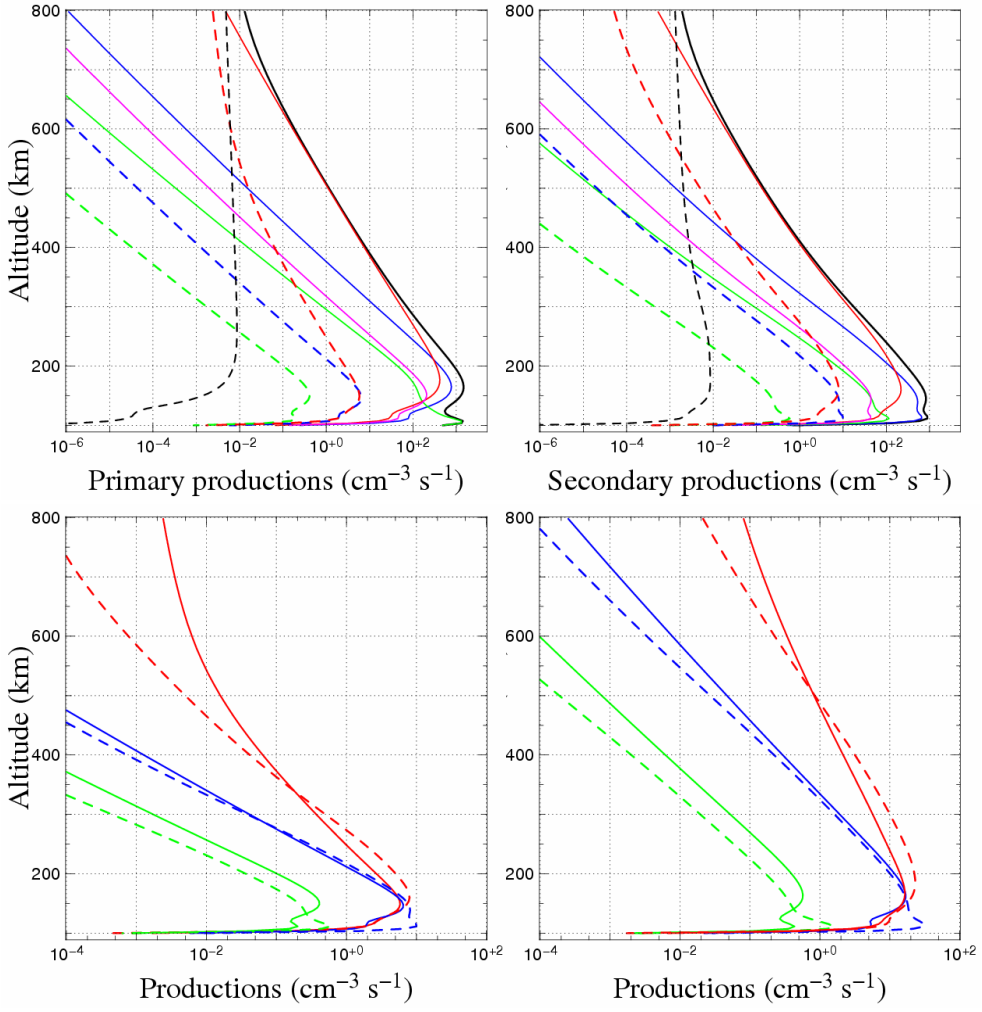

Fig. 5. Ion production profiles between 100 and 800 km (top left and right) at Grenoble, χ=63.51°. The electron contribution (black solid curve) is given by the weighted sum of all ion species: N_2^+ (solid blue), O_2^+ (solid green), O^+(solid red), N^+ (solid magenta), H^+ (dashed black), N_2^{++} (dashed blue), O_2^{++} (dashed green) and O^{++} (dashed red). Primary productions are shown on the left and secondary productions on the right. Bottom: doubly-charged ion primary productions (solid curves) versus secondary productions (dashed curves) in minimum solar conditions ($f_{10.7}$=68, left) and in active solar conditions ($f_{10.7}$=243, right). N_2^{++} profiles are in blue, O_2^{++} in green and O^{++} in red.

We can see that collisions with electrons are negligible whatever the altitude. The other plots underline the growing efficiency with altitude of the O^{++}+O mechanism: above 350 km, collisions with O play the major role in the final concentration shape and magnitude. We can then conclude that at lower altitudes, where collisions with N_2 and O_2 molecules are prominent, the model is almost not influenced by the O^{++}+O process. As this latter process is also subject to the largest uncertainties, the model verifies AE measurements better for altitudes being below 300 km. This low-altitude validity acts as a cornerstone to the overall validity of the model.

So far as we have access to very few satellite data and as there is a clear lack of statistics, our present photochemical model is validated over the range of altitudes 100–500 km for O^{++}. We have determined by means of a fit the charge-exchange reaction rate constant of O^{++} with O. Concerning N_2^{++} and O_2^{++}, ionosphere measurements have never been performed, and provided that our reaction rates are up to date and our modelling approach is similar to that of O^{++}, we can assume that the model is also valid for these two molecular dications. However, two strong limitations arise. First, due to the present lack of laboratory studies, it was not possible to take into account the reaction of molecular dications with O, although it is probably the major loss process at higher altitudes as we already showed for O^{++}. As a final step, we need direct data comparison to ascertain the hypotheses and look for the best geophysical conditions to create molecular ions in the ionosphere. In the next sections, a detailed sensitivity study of dication productions and densities is carried out.

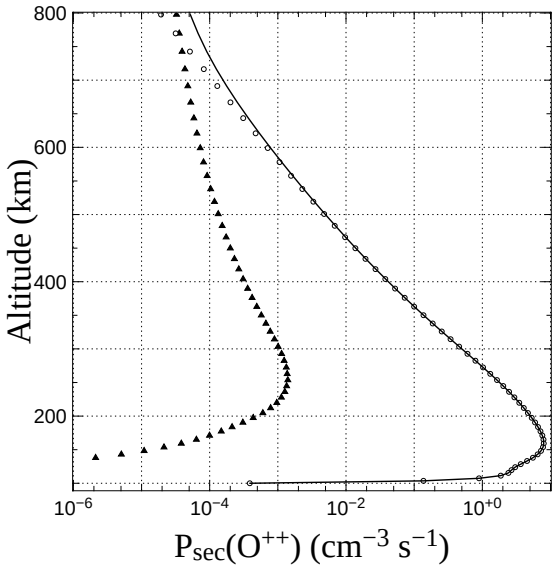

Fig. 6. Detail of the secondary productions of O^{++} in Grenoble and for quiet solar conditions, χ=63.51°. Productions of O^{++} via double ionisation by electron impact of O are shown in open circles. The single ionisation of O^+ is represented by black triangles. The solid curve is the total secondary production of O^{++} (in cm^{-3} s^{-1}) through both mechanisms.

5 Sensitivity study of productions and densities

Three main geophysical parameters are taken into account that are summarized in Table 5. Grenoble (France) is assumed to be representative of middle latitudes and Tromsø (Norway) is a typical high-latitude site. Two solar flux conditions are studied through the $f_{10.7}$ proxy variation, i.e. $f_{10.7}$=68 (solar minimum) and $f_{10.7}$=243 (solar active conditions). Finally, the sensitivity of each ion profile is examined throughout an entire day at Tromsø: the solar zenith angle dependence is examined in detail. All over this work the magnetic index A_p is set to 3, in order to avoid any influence from the magnetic activity. We choose day 120 of the year (early May) to compute our productions, losses and densities.

5.1 Primary and secondary productions

5.1.1 General considerations

Although the densities are computed only below 500 km, the production is of course calculated and shown up to 800 km. Primary and secondary production profiles of the main ion species are presented in Fig. 5 between 100 and 800 km.

The electron contribution is simply the weighted sum of all ion species: for dications, two electrons are produced for each double-ionization of a neutral species. Its production profile shows a two-peak shape particularly clear for the primary productions, one at low altitudes near 110 km (due to O_2^+), the other near 180 km (due to N_2^+ and O^+). The lower part of the figure shows the evolution of the dication productions under quiet (bottom left) and active solar flux conditions (bottom right).

The productions rates of a doubly-charged ion are smaller than those for singly-charged ions by a factor at least equal to 100. At very high altitudes, however (>600 km), the O^{++} primary production rate can represent up to 10% of that of O^+.

A change of dependence in O^{++} profiles is clearly seen on the left-hand side of Fig. 5, particularly sensitive for the primary productions. This evolution is interpreted as the two physical mechanisms causing the production of O^{++}, i.e. the double ionisation of O and the single ionisation of O^+, both through photoionisation and electron impact ionisation. The single photoionisation of O^+ is the prominent mechanism at high altitudes (400–800 km) while the double photoionisation of O plays the most important role at lower altitudes. Among the secondary production mechanisms (electron impact ionisation), the ionisation of O^+ is the major reaction for producing O^{++} ions from 700 km upwards, as shown in Fig. 6.

As stated in Lilensten et al. (1989) and seen in Fig. 5 (bottom), secondary dication productions contribute up to 30% of the total ion productions above 180 km and are the main contribution at lower altitudes (100–200 km for the molecular dications, 100–350 km for O^{++}), because of the photon penetration altitude into the ionosphere.

The difference between molecular dications and O^{++} is due both to the rather high double ionisation threshold of O (48.74 eV) and to the electron-impact cross sections that are 25 times larger than the double photoionisation cross sections of O.

5.1.2 Influence of the solar activity

In Fig. 5 (bottom), productions increase together with the solar flux index. The production rate peak increases in altitude from 150 km to 180 km from low to high solar activity. Between $f_{10.7}$=68 and $f_{10.7}$=243, their intensity increases by a mean factor of 2.5 at low altitudes, owing to the growth of neutral densities. Above 300 km, the solar flux intensification is more noticeable and production rates increase by a factor of 50 to 10^2 for $f_{10.7}$=243, from minimum to maximum solar activity.

5.1.3 Influence of the latitude

The effect of the latitude is much smaller, as neither the general shape nor the global low-altitude peak intensities of dication production rates are observed to change significantly when moving from middle latitudes (Grenoble) to high latitudes (Tromsø). The only effect that can be seen at Tromsø is an increase in the total production rate of molecular dications, and a slight decrease in the production rate of O^{++}. Differences between the two sites are less than 15% below 200 km for all three doubly-charged ions but can reach 50% for N_2^{++} and O_2^{++} at 600 km.

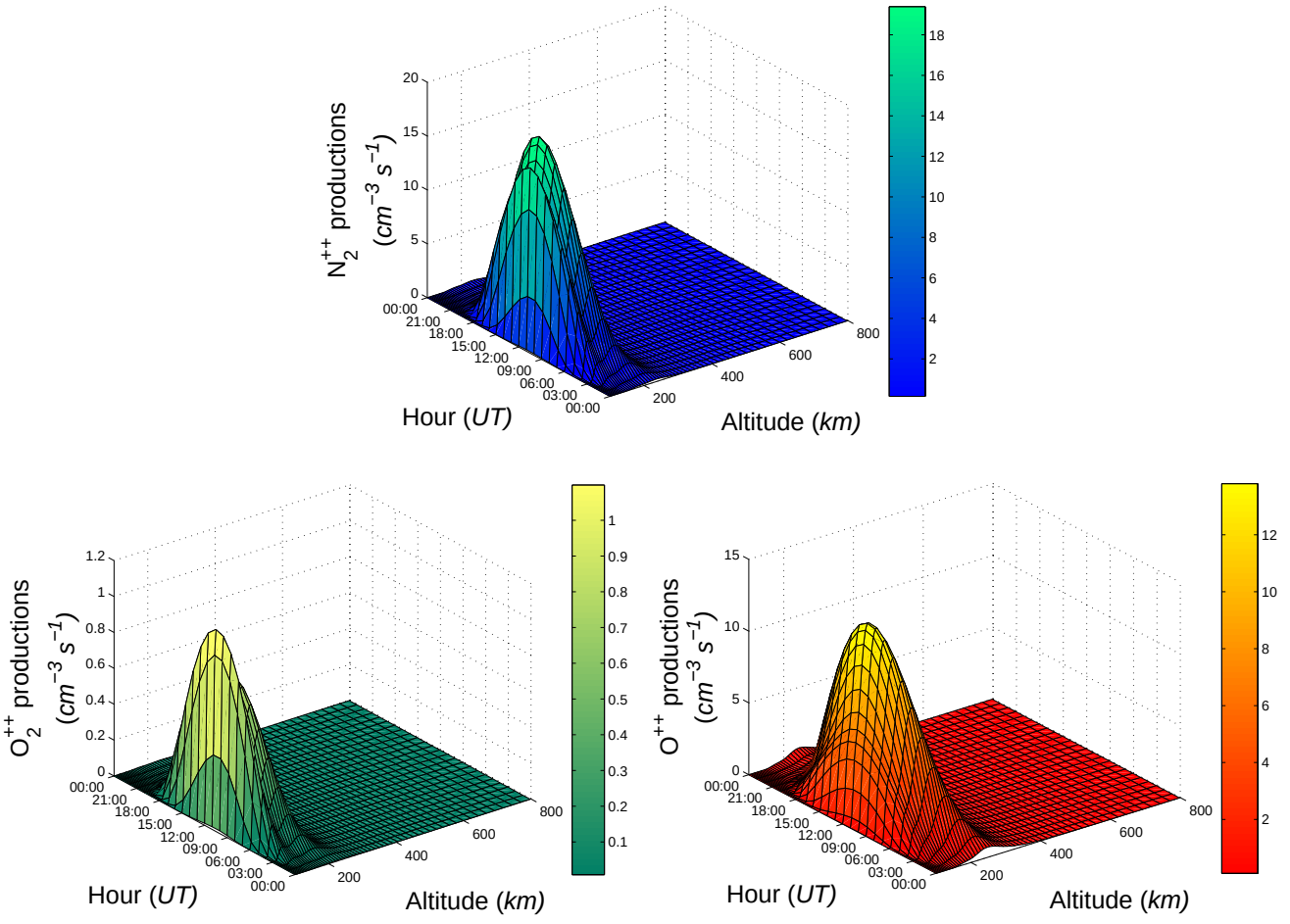

Fig. 7. Total productions (primary and secondary) of N_2^{++} (blue), O_2^{++} (green), O^{++} (red) over a whole day at Tromsø, for minimum solar flux conditions ($f_{10.7}$=68). Molecular dications show two sharp peaks at low altitudes, one around 115 km ascribed to the secondary production profiles, the other near 180 km attributed to the primary production profiles. O^{++} presents a wide peak around 220 km, mixing together the two production contributions.

5.1.4 Influence of the solar zenith angle

Together with the solar activity, the solar zenith angle variation is the parameter which has the strongest influence on productions. The larger the solar zenith angle, the more intense the solar flux absorption, because of the larger column density of atmosphere along the path of the photons: it implies that at a given altitude, fewer productions will be seen and the peaks will be shifted towards higher altitudes (Fig. 7). At χ=90°, for instance, and according to the model, no ions are produced at 100 km, regardless of the solar conditions.

This simple reasoning is verified for N_2^{++} and O_2^{++}. As seen in Fig. 7, peaks for molecular dications come in twos and are centred at very low altitudes (115 km and 120 km for N_2^{++} and O_2^{++}, respectively) due to secondary productions and the other at 180 km due to the primary production. O^{++} single production peak is wider and centred around 220 km, a difference due to the density of atomic oxygen which becomes prominent over N_2 and O_2, from 200 km upwards.

5.1.5 Brief summary

The cumulative contribution of these 3 ions can be up to 5% of the total primary electron production and more than 10% for the secondary electron production, depending on the solar flux conditions and the solar zenith angle. As seen before, the total ion production rate is the sum of primary and secondary production rates. In the altitude range considered, secondary production rates contribute 50% of the total O^{++}ion production rate. For N_2^{++}, it reaches an average value of 15%, and for O_2^{++} a value of less than 5%. According to the results of the model, O_2^{++} is the rarest produced species of all three dications by a factor of at least 10.

Figure 8 shows the total production above Tromsø for all eight ions at minimum solar activity conditions and for χ=63.51°. Two peaks are visible for N_2^{++} and O_2^{++}, one around 110 km, the other at 180 km. For O^{++}, the

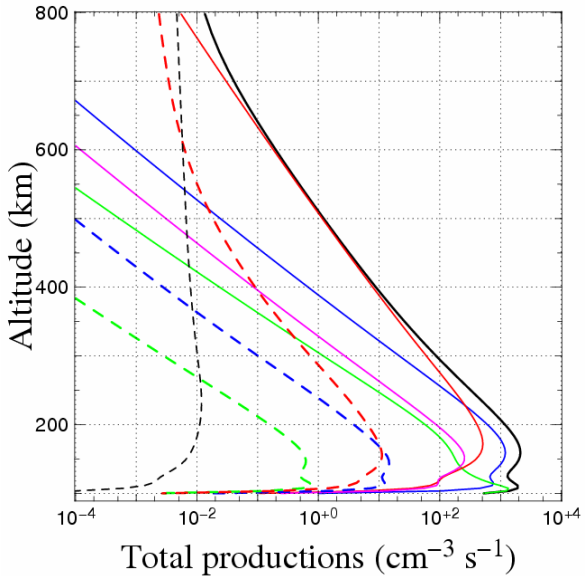

Fig. 8. Total ion productions at Tromsø, $f_{10.7}$=68, for the ions N_2^+ (solid blue), O_2^+ (solid green), O^+(solid red), N^+(solid magenta), H^+(dashed black), N_2^{++} (dashed blue), O_2^{++} (dashed green) and O^{++} (dashed red). The total electron productions are represented in solid black.

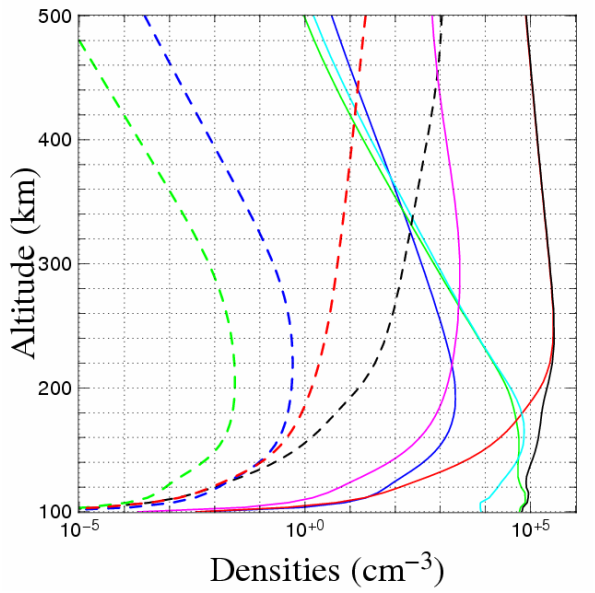

Fig. 9. Density profiles of the major ionic species in the ionosphere above Tromsø, $f_{10.7}$=68 and at χ=63.51. N_2^+ is plotted in solid dark blue, O_2^+ in solid green, O^+in solid red, N^+in magenta, H^+in dashed black, NO^+in solid light blue, N_2^{++} in dashed blue, O_2^{++} in dashed green and O^{++} in dashed red. The electron density is represented in black solid. The three doubly-charged ion densities are computed under the photochemical equilibrium assumption.

production reaction $O^+ + h\nu \rightarrow O^{++} + e^-$ becomes prominent above 500 km and leads to a more slowly decreasing slope for the total production.

5.2 Densities

Figure 9 shows the major ion densities above Tromsø, for the minimum solar activity model. Near 160 km, the F_1 ionospheric layer is clearly seen, characterised by a peak in NO^+ density. We plot the electron density in black. Doubly-charged ions are represented by dashed lines.

We note that, among dications, the highest densities are expected for O^{++} which reaches 60 to 100 ions per cm^3 at 500 km, and becomes the ion with the fourth highest density, after O^+, H^+ and N^+. At 500 km, the O^{++} density is 10^5 times larger than N_2^{++} and O_2^{++}. Peaks in the density of N_2^{++} and O_2^{++} (1 cm^{-3} and 0.01 cm^{-3}, respectively) are then predicted between 200 km and 250km.

5.2.1 Solar flux effect

O^{++} densities increase by a factor of 2.5 between 150 and 500 km, from low ($f_{10.7}$=68) to high ($f_{10.7}$=243) solar activity (Fig. 10, top). At the same time, N_2^{++} densities increase by a factor of 3 between 100 and 300 km, and by an increasing factor of 10 to 10^5 above 300 km. O_2^{++} follows the same evolution as N_2^{++}: a mean factor 2 separates the two solar flux results between 100 and 200 km, while above 300 km, the factors by which the densities increase reach 10^5, showing that the differences become dramatically larger when altitudes increase.

5.2.2 Latitude influence

The influence of latitude is shown in Fig. 10 (bottom left). Generally speaking, the densities are more important at high latitudes for N_2^{++} and O_2^{++} whereas it is the opposite for O^{++}. The differences are ranging from a constant 40% for O^{++} to a highly variable factor for N_2^{++} and O_2^{++} depending on the solar conditions and the altitude (less than 10% at low altitudes or for active solar conditions, continuously-increasing in quiet conditions above 250 km, eventually reaching 40% at 500 km).

5.2.3 Solar zenith angle evolution

In Fig. 10 (bottom right), we consider two extreme cases to study the solar zenith angle effect on dication densities at mean latitude: local zenith (χ=30.47°), and twilight (χ=90°). Significant changes at low altitudes are to be seen for χ=90°: peaks appear higher in altitude and their amplitude drops on average by a factor of 1.5.

Around 500 km, O^{++} densities are slightly larger for twilight conditions, a tendency which does not recur with molecular doubly-charged ions. This original feature results from a more efficient O^{++} production at high altitudes, as explained in the previous section.

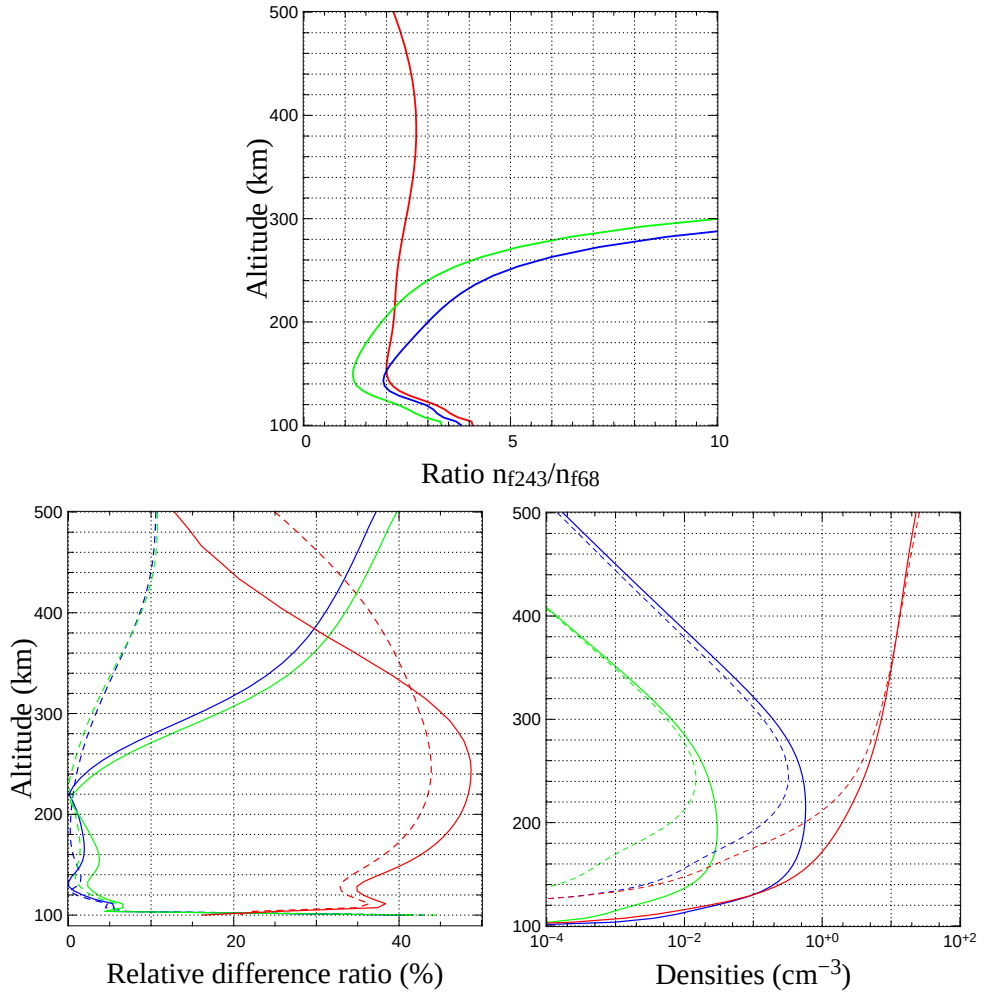

Fig. 10. Solar flux (top panel), latitudinal (bottom left panel) and solar zenith angle (bottom right panel) variation influences on dication densities. Top: we plot the ratio $\frac{n_i(f_{10.7}=243)}{n_i(f_{10.7}=68)}$ above Grenoble, χ=63.51°. N_2^{++} is in blue, O_2^{++} in green and O^{++} in red. Bottom left: latitudinal relative differences between Tromsø and Grenoble are shown for each three species N_2^{++} (blue), O_2^{++} (green) or O^{++}(red) in active (dashed curves) and quiet (solid curves) solar conditions. Bottom right: densities of the three dications for χ=30.94° (solid curves) and for χ=90° (dashed curves).

6 Detection of doubly-charged ions in planetary ionospheres

Two methods are available, namely mass spectrometers experiments and optical measurements.

6.1 Mass spectrometers

Originally, mass spectrometer experiments were the first device used on board satellites to yield some information about the ion composition of the atmosphere. Thus, Atmosphere Explorer and Pioneer were used to look for doubly-charged ions in the atmosphere of the Earth and Venus. With the Cassini-Huygens mission to the Saturnian system, much effort has been produced most recently to obtain a proper atmosphere/ionosphere model of Titan to be made available to the community. Predictions have then been cast on the possible existence of doubly-charged species in Titan's ionosphere (Lilensten et al., 2005a and 2005b).

This technique allows for the quantitative detection of a given ion through its mass to charge ratio m/q.

On Earth, the determination of O^{++} (m/q=8) is particularly easy because it does not overlap with other species. However, this method is not suitable for molecular dications such as N_2^{++} and O_2^{++} as N^+ and O^+ have, respectively, the same mass to charge ratio.

According to the present model, the detection of the three dications, N_2^{++}, O_2^{++} and O^{++}, will be made easier in solar maximum conditions and at noon when densities are at their highest. Latitude is not a crucial parameter and should not be worried about when recording data in the ionosphere.

Table 6. Fluorescence wavelengths and transitions for N_2^{++}, O_2^{++} and O^{++}.

Species	l (nm)	Transition
N_2^{++}	158.9 – 159.4	(1,1) band
	158.7 – 159.3	$D\,^1\Sigma_u^+(0) \rightarrow X\,^1\Sigma_g^+(0)$
O^{++} (OIII)	500.824	$^1D_2 \rightarrow {}^3P_2$ **N1**
	496.029	$^1D_2 \rightarrow {}^3P_1$ **N2**
	436.443	$^1S_0 \rightarrow {}^1D_2$
	232.166	$^1S_0 \rightarrow {}^3P_1$
	166.615	$^5S_2{}^0 \rightarrow {}^3P_2$
	166.081	$^5S_2{}^0 \rightarrow {}^3P_1$
O_2^{++}	470	$A\,^3\Sigma_u^+ - X\,^1\Sigma_u^+$
	443	
	417	

6.2 Spectroscopy of dications

Among doubly-charged ions, N_2^{++} has perhaps been the most widely studied species for over two decades. The ground state of N_2^{++}, denoted by $X^1\Sigma_g^+$, is 43.00 eV above the ground neutral state (Ahmad, 2002, see Table 1). So far, 8 excited electronic states have been identified, such as the first ones $a^3\Pi_u$ and $b^3\Sigma_g^-$, situated at 0.57 and 1.48 eV, respectively, above the N_2^{++} ground state (Taylor and Partridge, 1987). The ground state $X^1\Sigma_g^+$ of O_2^{++} is located at 36.13 eV above the ground neutral state, and the first excited state $A^3\Sigma_u^+$ at 4.16 eV above the O_2^{++} ground state (Fournier et al., 1992). Moreover, the O_2^{++} vibrational structure has been investigated by a threshold photoelectron coincidence technique (TPESCO) (Hall et al., 1992 and references therein).

The O^{++} ground state $^3P_0$ is situated 48.74 eV above its ground neutral state (He et al., 1995). Many excited states exist, among which $^1D_2$, $^1S_0$ and $^5S_0^2$ lie 2.513 eV, 5.354 eV and 7.479 eV, respectively, above the O^{++} ground level. These states are notably involved in the formation of emission lines, discussed in the next paragraph.

6.3 Fluorescence

The fluorescence of O^{++} is well-known since its doublet centred around 500 nm has been used as a tracer of electron densities and temperatures in gaseous nebulae since the 1940s (e.g. Menzel and Haller, 1941).

Due to the fast dissociation or predissociation of molecular dication excited states, fluorescence towards the ground state is generally a rare phenomenon, but was at least observed for N_2^{++} (Cossart et al., 1985; Cossart and Launay, 1985; Olsson et al., 1988; Ehresmann et al., 2000). For O_2^{++}, Avakyan (1978b) also reports the possible identification of auroral emissions around 243 nm which he ascribes to the $A^3\Sigma_u^+$–$X^1\Sigma_g^+$ transition: despite the fact that no further confirmation of a fluorescence feature in O_2^{++} has yet been found, three emission wavelengths have recently been tabulated by Avakyan (1998), as shown in Table 6, where we list the fluorescence transitions and their respective wavelengths for N_2^{++}, O_2^{++} and O^{++}. The O^{++} transitions are situated in the visible blue spectrum and in the UV range.

The $N_()$ excited state of specific interest to us is $D^1\Sigma_u^+$, which lies 7.8 eV above the N_2^{++} ground state (Ahmad, 2002; Olsson et al., 1988). This state fluoresces in transitions to the N_2^{++} ground state, with bands centred around 159 nm (Table 6). The fluorescence lifetime of the $N_2^{++}\,D^1\Sigma_u^+$ electronic state is 6.0±0.5 ns, according to Olsson et al. (1988). No collisional deactivation is therefore liable to occur in the ionosphere during this very short lifetime. Using the results of Ehresmann et al. (2003), a rough approximation leads us to conclude that nearly 10% of the total N_2^{++} ions created by double photoionisation at the cross-section peak near 65 eV, are produced in this state. As densities for N_2^{++} reach, at the most, 1 ion per cm^3, we would expect, in a very optimistic hypothesis, that a mere 0.1 ion per cm^3 is produced in the fluorescent state. Depending on the solar flux intensity, we can then estimate the maximum intensity likely to be produced along the line of sight by integrating ion productions over our altitude range. The intensity ranges from 0.6 R in quiet solar conditions to 2.3 R in active solar conditions. This value is high enough to be detected by spectrophotometers whose accuracy lies typically within the sub deci-Rayleigh range.

Regarding O^{++}, it is by far the most abundant doubly-charged species in the Earth's ionosphere and is therefore the most likely to be detected optically in aurora or diurnal high-resolution spectra. Besides the forbidden transitions N_1 and N_2, three other lines exist for O^{++} in the UV range (see Table 6; NIST database at http://physics.nist.gov/cgi-bin/AtData/main_asd) but have never been identified in the diurnal ionosphere spectrum. The radiative lifetime of the $^5S_2^0$ metastable level of O^{++} was measured to be 1.22±0.08 ms (Johnson et al., 1984). A fruitful comparison with mass spectrometer results on board satellites should be of great interest in the years to come.

7 Conclusion and perspectives

Throughout this work, we study the densities of stable, doubly-charged ions produced in the Earth's dayside ionosphere. For the first time a comprehensive investigation of the problem is led for N_2^{++}, O_2^{++} and O^{++}. The photokinetic model TRANSCAR, based on Boltzmann's formalism, is used to yield productions (primary and secondary). In order to compute the densities of each doubly-charged ion, a photochemical part is built up in which reaction rate constants are included. The main inputs of the model are given

by laboratory experiments. Emphasis is laid on the need for laboratory measurements concerning double photoionisation cross sections of N_2 and O_2, as well as the reactions of dications with O.

We then validate our approach for O^{++} by the comparison with the only measurements available, those recorded by the satellite Atmosphere Explorer in the mid-seventies. The reaction rate constant concerning the $O^{++}+O \rightarrow O^{+}+O^{+}$ reaction is predicted to be $1.06\pm0.40\times10^{-10}$ cm^3 s^{-1} and needs to be confirmed by laboratory experiments.

A sensitivity study is also proposed, showing the most favourable conditions for the productions and existence of doubly-charged ions, via the variation of the solar flux intensity (high $f_{10.7}$), the geographical coordinates (middle latitudes) and the solar zenith angle (local zenith).

More comparisons with satellite data should, of course, be carried out in the future, both by measurements of the diurnally varying spectra (need of high resolution spectra) and by mass spectrometers on board satellites.

To bring this study to a conclusion, the effects of solar-wind precipitations could be investigated.

This study is the third of a series of predictions undertaken on Mars (Witasse et al., 2002), Titan (Lilensten et al., 2005a and 2005b) and the Earth. Together with the work performed by Fox and Victor (1981) on Venus and Brown et al. (1983) on Io, we can suggest that doubly-charged ions are a common feature of planets and satellites with thick atmospheres.

Acknowledgements. C. S. thanks M. Barthélemy and F. Culot (LPG) for fruitful discussions throughout the building of this work.

Topical Editor M. Lester thanks J. Fox and S. V. Avakyan for their help in evaluating this paper.

References

Aguilar, A., Covington, A. M., Hinojosa, G., Phaneuf, R. A., Álvarez, I., Cisneros, C., Bozek, C. D., Dominguez, I., Sant'Anna, M. M., Schlachter, A. S., Nahar, S. N., and McLaughlin, B. M.: Absolute photoionization cross section measurements of OII ions from 29.7 to 46.2 eV, Ap. J. S., 146, 467–477, 2003.

Ahmad, M.: Dynamique et dissociation des dications N_2^{++} et NO_2^{++} préparés par double photoionisation à l'aide du rayonnement synchrotron, PhD thesis, Université Paris VI, 2002.

Aitken, K. L. and Harrison, M. F. A.: Measurement of the cross sections for electron impact ionization of multi-electron ions: I. O^+ to O^{2+} and O^{2+} to O^{3+}, J. Phys. B: Atom. Molec. Phys., 4, 1176–1188, 1971.

Angel, G. C. and Samson, J. A. R.: Total photoionization cross sections of atomic oxygen from threshold to 44.3 Å, Phys. ReV.*A*, 58, No. 11, 5578–5585, 1988.

Aston, F. W., Philos. Mag., 40, 628–634, 1920, quoted in: Seiersen et al., Dissociative recombination of dications, J. Chem. Phys., 119, No. 2, 2003.

Avakyan, S. V.: Doubly charged ions of atomic oxygen in the disturbed ionosphere, Cosmic Res., 16, No. 1, 115–119, 1978a.

Avakyan, S. V.: Doubly charged molecular ions in the auroral ionosphere, Geomag. Aeron., 18, No. 4, 444–446, 1978b.

Avakyan, S. V.: Formation of doubly-charged ions of atomic oxygen in the upper atmosphere, Cosmic Res., 17, No. 6, 942–943, 1980.

Avakyan, S. V.: Auger processes in the optics of the upper atmosphere, J. Opt. Technol., 65, No. 11, 870–875, 1998.

Bahati, E. M., Jureta, J. J., Belic, D. S., Cherkani-Hassani, H., Abdellahi, M. O., and Defrance, P.: Electron-impact dissociation and ionization of N_2^+, J. Phys. B: At. Mol. Opt. Phys., 34, 2963–2973, 2001.

Baluja, K. L. and Zeippen, C. J.,: The photoionisation of the $O^+(^4S^0)$ ground state, J. Phys. B: At. Mol. Opt. Phys., 21, 2441–2454, 1988.

Breig, E. L., Torr, M. R., and Kayser, D. C.: Observations and photochemistry of O^{++} in the daytime thermosphere, J. Geophys. Res., 87, No. A9, 7653–7665, 1982.

Breig, E. L., Torr, M. R., Torr, D. G., Hanson, W. B., Hoffman, J. H., Walker, J. C. G., and Nier, A. O.: Doubly charged atomic oxygen ions in the thermosphere 1. Photochemistry, J. Geophys. Res., 82, No. 7, 1008–1012, 1977.

Brown, R. A., Shemansky, D., and Johnson, R. E.: A deficiency of OIII in the Io plasma torus, Ap. J., 264, 309–323, 1983.

Chatterjee, B. K. and Johnsen, R.: Thermal-energy reactions of O_2^{++} ions with O_2, N_2, CO_2, NO and Ne, J. Chem. Phys., 91, No. 2, 1378–1379, 1989.

Cossart, D., Launay, F., Robbe, J. M., and Gandara, G. J.: The optical spectrum of the doubly charged molecular nitrogen ion-rotational analysis of the (0–0) and (1–1) bands of the $D^1\Sigma_u^+$–$X^1\Sigma_g^+$ transition of N_2^{++}: comparison of observations with ab-initio calculatio results, J. Mol. Spectrosc., 113, 142–158, 1985.

Cossart, D. and Launay, F.: The vacuum UV emission spectrum of the $^{15}N_2^{2+}$ molecular ion, J. Mol. Spectrosc., 113, 159–166, 1985.

Cox, S. G., Critchley, A. D. J., Kreynin, P. S., McNab, I. R., Shiell R. C., and Smith, F. E.: High resolution spectroscopy and structure of molecular dications, Phys. Chem. Chem. Phys., 5, No. 4, 663–676, 2003.

Ehresmann, A., Liebel, H., Schmoranzer, H., Zimmermann, B., Kammer, S., Schartner, K.-H., Demekhin, Ph. V. and Sukhorukov, V. L.: Double photoionization of N_2 into the N_2^{++} $D^1\Sigma_u^+$-state, J. Phys. B: At. Mol. Opt. Phys., 36, 3669–3681, 2003.

Ehresmann A., Machida, S., Kitajima, M., Ukai, M., Kameta, K., Kouchi, N., Hatano, Y., Shigemasa, E., and Hayaishi, T.: Dissociative single and double photoionization with excitation between 37 and 69 eV in N_2, J. Phys. B: At. Mol. Opt. Phys., 33, 473–490, 2000.

Fang, Z. and Kwong, V. H. S.: Charge transfer between the $2p^2\ ^3$P ground-state O^{2+} ion and He, H_2, N_2, and CO at electron-volt energies, Phys. Rev. A 51, No. 2, 1321–1326, 1995.

Fennelly, J. A. and Torr, D. G.: Photoionization and photoabsorption cross sections of O, N_2, O_2 and N for aeronomic calculations, At. Dat. Nucl. Dat. Tab., 51, 321–363, 1992.

Fournier, J., Fournier, P. G.: Langford, M. L., Mousselmal, M., Robbe, J. M., and Gandara, G.: An experimental and theoretical study of the doubly-charged ion O_2^{++}, J. Chem. Phys., 96, No. 5, 3594–3602, 1992.

Fox, J. L. and Victor, G. A.: O^{++} in the Venusian ionosphere, J. Geophys. Res., 86, No. A4, 2438–2442, 1981.

Franceschi, P., Thissen, R., Zabka, J., Roithova, J., Herman, Z., and Dutuit, O.: Internal energy effects in the reactivity of CO_2^{2+} doubly charged molecular ions with CO_2 and CO, Int. J. Mass Spectrom., 228, 507–516, 2003.

Geiss J. and Young, D. T.: Production and Transport of O^{++} in the ionosphere and plasmasphere, J. Geophys. Res., 86, No. A6, 4739–4750, 1981.

Glosik, J., Rakshit, A. B., Twiddy, N. D., Adams, N. G., and Smith, D.: Measurement of the rates of reaction of the ground and metastable excited states of O_2^+, NO^+ and O^+ with atmospheric gases at thermal energies, J. Phys. B: Atom. Molec. Phys., 11, No. 19, 3365–3379, 1978.

Halas, S. and Adamczyk, B.: Cross sections for the production of N_2^+, N^+ and N_2^{++} from nitrogen by electrons in the energy range 16–600 eV, Int. J. Mass Spectrom. Ion Phys., 10, 157–160, 1972.

Hall, R. I., Dawber, G., McConkey, A., MacDonald, M. A., and King, G. C.: Vibrational structure of the O_2^{++} ground state observed by threshold photoelectron coincidence spectroscopy, Phys. ReV. Lett., 68, No. 18, 2751–2754, 1992.

Hardy, D. A., Gussenhoven, M. S., Raistrick, R. and McNeil, W. J.: Statistical and functional representations of the pattern of auroral energy flux, number flux and conductivity, J. Geophys. Res., 92, No. A11, 12 275–12 294, 1987.

He, Z. X., Moberg, R., and Samson, J. A. R.: Threshold behaviour in single-photon double ionisation of atomic oxygen, Phys. ReV. A: At. Mol. Opt. Phys., 52, No. 6, 4595–4598, 1995.

Hedin, A. E.: MSIS-86 Thermospheric model, J. Geophys. Res., 92, No. A5, 4649–4662, 1987.

Hedin, A. E.: Extension of the MSIS thermosphere into the middle and lower thermosphere, J. Geophys. Res., 96, 1159–1172, 1991.

Hellner, L., Besnard, M. J., and Dujardin, G.: Photoionization study of quasibound states of doubly charged molecular nitrogen ions, Chem. Phys., 119, 391–397, 1988.

Heroux, L. and Hinteregger, H.E.: Aeronomical reference spectrum for solar UV below 2000 Å, J. Geophys. Res., 83, No. A11, 5305–5308, 1978.

Hoffman, J. H.: Composition measurements of the topside ionosphere, Science, 115, 322–324, 1967.

Hoffman, J. H., Hanson, W. B., Lippincott, C. R., and Ferguson, E. E.: The magnetic ion-mass spectrometer on Atmosphere Explorer, Radio Sci., 8, 315–322, 1973.

Horwitz, J. L.: ISEE 1 observations of O^{++} in the magnetosphere, J. Geophys. Res., 86, No. A11, 9225–9229, 1981.

Howorka, F., Viggiano, A. A., Albritton, D. L., Ferguson, E. E., and Fehsenfeld, F. C.: Laboratory studies of O^{++} reactions of ionospheric importance: J. Geophys. Res., 84, No. A10, 5941–5942, 1979.

Itikawa, Y. and Ichimura, A.: Collisions of electrons and photons with atomic oxygen, J. Phys. Chem. Ref. Data, 19, No. 3, 637–651, 1990.

Johnsen, R. and Biondi, M. A.: Measurements of the reaction rates of O^{++} ions with N_2 and O_2 at thermal energy and their ionospheric implications, Geophys. Res. Lett., 5, No. 10, 847–848, 1978.

Johnson, B. C., Smith, P. L., and Knight, R. D.: The radiative lifetime of the $^5S_2^0$ metastable level of O^{++}, Ap. J., 281, 477–481, 1984.

Kjeldsen, H., Kristensen, B., Brooks, R. L., Folkmann, F., Knudsen, H., and Andersen, T.: Absolute, state-selective measurements of the photoionization cross sections of N^+ and O^+ ions, Astrophys. J. supplement series, 138, 219–227, 2002.

Krishnakumar, E. and Srivastava, S. K.: Cross sections for the production of N_2^+, N^++N_2^{++} and N^{2+} by electron impact on N_2, J. Phys. B.: At. Mol. Opt. Phys., 23, 1893–1903, 1990.

Krishnakumar, E. and Srivastava, S. K.: Cross sections for electron impact ionization of O_2, Int. J. Mass Spectrom. Ion Proc., 113, 1–12, 1992.

Lilensten, J. and Blelly, P.-L.: The TEC and F2 parameters as tracers of the ionosphere and thermosphere, J. Atmos. Solar and Terrest. Phys., 64, 775–793, 2002.

Lilensten, J., Kofman, W., Wisemberg, J., Oran, E. S. and Devore, C. R.: Ionization efficiency due to primary and secondary photoelectrons: a numerical model, Ann. Geophys., 7, 83–90, 1989.

Lilensten, J., Simon, C., Witasse, O., Dutuit, O., Thissen, R. and Alcaraz, C.: A fast computation of the diurnal ion production in the ionosphere of Titan, accepted in Icarus, 2005a.

Lilensten, J., Witasse, O., Simon, C., Soldi-Lose, H., Dutuit, O., Thissen, R., and Alcaraz, C.: Prediction of a N_2^{++} layer in the upper atmosphere of Titan, Geophys. Res. Lett., 32, L03203, 2005b.

Mrázek, L., Zabka, J., Dolejsek, Z., Hrusak, J., and Herman, Z.: Dynamics of chemical and charge-transfer reactions of molecular dications: III Beam scattering and total cross section data for processes in system $CO_2^{++}+D_2$, J. Phys. Chem. A, 104, 7294–7303, 2000.

Mathur D., Andersen, L. H., Hvelplund, P., Kella, D., and Safvan, C. P.: Long-lived, doubly charged diatomic and triatomic molecular ions, J. Phys. B: At. Mol. Opt. Phys., 28, 3415–3426, 1995.

Meinel, A. B.: The spectrum of the airglow and the aurora, Rep. Prog. Phys., 14, 121–146, 1951.

Menzel, D. H. and Aller, L. H.: Physical Processes in gaseous nebulae. XVI. The abundance of OIII, Ap. J., 94, 30–36, 1941.

Morel, L., Witasse, O., Warnant, R., Cerisier, J.-C., Blelly, P.-L., and Lilensten, J.: Diagnostic of the dayside ionosphere of Mars using the Total Electron Content measurement by the NEIGE/Netlander experiment: an assessment study, Planet. Space Sci., 52, No. 7, 603–611, 2004.

Märk, T. D.: Cross sections for single and double ionization of N_2 and O_2 molecules by electron impact from threshold up to 170 eV, J. Chem. Phys., 63, No. 9, 3731–3736, 1975.

Nakada, M. P. and Singer, S. F.: Thermal diffusion and multiply-charged atoms in the magnetosphere, Geophys. J. Roy. astr. Soc., 15, 163–181, 1968.

Nicolas, C., Alcaraz, C., Thissen, R., Zabka, J., and Dutuit, O.: Effects of ion excitation on ion-molecule reactions of the Mars, Venus, and Earth ionospheres, Planet. Space Sci., 50, 877–887, 2002.

Olsson, B. J., Kindvall, G., and Larsson, M.: Experimental and theoretical studies of the radiative properties of the $N_2^{++}D^1\Sigma_u^+$ state, J. Chem. Phys., 88, No. 12, 7501–7507, 1988.

Prasad, S. S. and Furman, D. R.: On the importance of doubly-charged ions in the auroral ionosphere, J. Geophys. Res., 80, 1360–1362, 1975.

Seiersen, K., Heber, O., Jensen, M. J., Safvan, C. P. and Andersen, L. H.: Dissociative recombination of dications, J. Chem. Phys., 119, No. 2, 2003.

Smith, D. and Adams, N. G.: Elementary plasma reactions of environmental interest, Topics Curr. Chem., 89, 1–43, 1980.

Straub, H. C., Renault, P., Lindsay, B. G., Smith, K. A., and Stebbings, R. F.: Absolute partial cross sections for electron-impact ionisation of H_2, N_2 and O_2 from threshold to 1000 eV, Phys. ReV.*A*, 54, No. 3, 2146–2152, 1996.

Swartz, W. E. and Nisbet, J. S.: Revised calculations of the F region ambient electron heating by photoelectrons, J. Geophys. Res., 77, 6259–6261, 1972.

Taylor, P. R. and Partridge, H.: Theoretical determination of the ground state of N_2^{++}, J. Phys. Chem., 91, No. 24, 6148–6151, 1987.

Thomson, J. J.: Rays of positive electricity and their application to chemical analysis, 2nd ed., Longmans Green and Co., London, 1921.

Tobiska, W. K.: Revised solar extreme ultraviolet flux model, J. Atmos. Terrest. Phys., 53, No. 11/12, 1005–1018, 1991.

Victor, G. A and Constantinides, E. R.: Double photoionization and doubly charged ions in the thermosphere, Geophys. Res. Lett., 6, No. 6, 519–522, 1979.

Walker, J. C. G.: The density of O^{2+} ions in the topside ionosphere, Planet. Space Sci., 18, 559–564, 1970.

Witasse, O.: Modélisation des ionosphères planétaires et de leur rayonnement : la Terre et Mars, PhD thesis, UJF/CNRS, Université Grenoble I, 2000.

Witasse, O., Dutuit, O., Lilensten, J., Thissen, R., Zabka, J., Alcaraz, C., Blelly, P.-L., Bougher, S. W., Engel, S., Andersen, L. H., and Seiersen, K.: Prediction of a CO_2^{++} layer in the atmosphere of Mars, Geophys. Res. Lett., 29, No. 8, 104-1, 2002.

Witasse, O., Dutuit, O., Lilensten, J., Thissen, R., Zabka, J., Alcaraz, C., Blelly, P.-L., Bougher, S. W., Engel, S., Andersen, L. H., and Seiersen, K.: Correction to "Prediction of a CO_2^{++} layer in the atmosphere of Mars", Geophys. Res. Lett., 30, No. 7, 12–1, 2003.

Yamada, I., Danjo, A., Hirayama, T., Matsumoto, A., Ohtani, S., Suzuki, H., Tawara, H., Takayanagi, T., Wakiya, K., and Yoshino, M.: Electron impact ionization of O^+, S^+ and S^{2+} ions, J. Phys. Soc. Jpn., 57, No. 8, 2699–2704, 1988.

Young, D. T., Geiss, J., Balsiger, H., Eberhardt, P., Ghielmetti, A., and Rosenbauer, H.: Discovery of He^{2+} and O^{2+} ions of terrestrial origin in the outer magnetosphere Geophys. Res. Lett., 4, No. 12, 561–564, 1977.

Ziegler, D. L., Newman, J. H., Smith, K. A., and Stebbings, R. F.: Double ionisation of atomic oxygen by electron impact, Planet. Space Sci., 30, No. 5, 451-456, 1982.

Zipf, E. C.: The ionisation of atomic oxygen by electron impact, Planet. Space Sci., 33, No. 11, 1303–1307, 1985.